Some Observations on Thermodynamic Basis of Pressure Continuum Condition and Consequences of Its Violation in Discretised CFD

A. W. Date

Nomenclature

A_k, AP	Coefficients in Discretised Equations
D	Mass Diffusivity
F	Volume Fraction
Fr	Froude Number
F_{st}	Surface Tension Force
g	Gravity Acceleration
k	Thermal Conductivity
Kn	Knudsen Number
Pc	Peclet Number
p	Pressure
q	Continuum-Preserving Stress/Pressure
R	Residual or Gas Constant
Re	Reynolds Number
Ra	Rayleigh Number
t	Time
u_i	Velocity in x_i, $i = 1, 2, 3$ direction
V	Volume
$\vec{V}$	Total Velocity Vector
We	Weber Number

A. W. Date (✉)
Mechanical Engineering Department, IIT Bombay, Mumbai 400076, India
e-mail: awdate@me.iitb.ac.in

A. Runchal (ed.), *50 Years of CFD in Engineering Sciences*,
https://doi.org/10.1007/978-981-15-2670-1_2

Greek Symbols

α, β	Under-Relaxation Factors
γ	Second viscosity coefficient
μ	Dynamic viscosity
ρ	Density
σ	Surface Tension Coefficient or Stress
τ	Stress

Suffixes

a	Refers to Heavier Fluid
b	Refers to Lighter Fluid or to Boundary Node
cont	Refers to continuum
disc	Refers to discretised space
f	Refers to CV Face Location
i	In i-direction
m	Refers to mass conservation or to mixture
n	Normal to the Interface
sm	Refers to Smoothing
th	Thermodynamic
x_i	Refers to x_i, $i = 1, 2, 3$ directions

Superscripts

l	Iteration Number
o	Refers to old time
$u_i, u_{f,i}$	Refers to Momentum Equation
$-$	Refers to Multidimensional Average
$'$	Refers to Correction

Acronyms and Short Forms

CV	Control Volume
CFD	Computational Fluid Dynamics
$F(\ )$	Function of
LS	Level-Set Method
VOF	Volume of Fluid Method

1 Introduction

1.1 Navier–Stokes Equations

In the study of transport in moving fluids, the fundamental laws of motion (conservation of mass and Newton's second law of motion) are applied to an elemental fluid. Two approaches are possible: (a) Particle approach and (b) Continuum approach.

In the *particle approach*, the fluid is assumed to consist of particles (molecules, atoms) and the laws are applied to study particle motion. Fluid motion is then described by statistically averaged motion of a group of particles. For most applications arising in engineering and the environment, however, this approach is too cumbersome[1] because the significant dimensions of the flow are considerably bigger than the mean free path length between molecules. In the *continuum approach*, therefore, statistical averaging is assumed to have been *already performed* and the fundamental laws are applied to portions of fluid (or *control volumes*) that contain a large number of particles. The information *lost in averaging* must, however, be *recovered*. This is done by invoking some further *auxiliary laws* and by empirical specifications of *transport properties* such as viscosity (μ), thermal conductivity (k) and mass diffusivity (D). The transport properties are typically determined from experiments. Notionally, the continuum approach is very attractive because one can now speak of temperature, pressure or velocity *at a point* and relate them to what is *measured* by most practical instruments.

Guidance for deciding whether particle or continuum approach is to be used can be had from *Knudsen number* $Kn = l/L$, where l is the mean free path length between molecules and L is a characteristic dimension (say, the radius of a pipe) of the flow. When Kn is very small ($<10^{-4}$), continuum approach is considered valid. In macro-engineering and environmental flows, therefore, continuum approach is adopted.

Control Volume (CV): *The CV may be defined as a region in space across the boundaries of which matter, energy and momentum may flow, and it is a region within which source or sink of the same quantities may prevail. Further, it is a region on which external forces may act.*

The Navier–Stokes equations are derived by applying the law of conservation of mass and Newton's second law of motion to a CV shown in Fig. 1. The CV having dimensions Δx_1, Δx_2 and Δx_3 is located at (x_1, x_2, x_3) from a fixed origin. The statements of the laws yield *algebraic equations* of mass and momentum conservation. These statements are then *converted* to *partial differential equations* by letting Δx_1, Δx_2 and $\Delta x_3 \rightarrow 0$ followed by invoking the mathematical definition of a derivative in a continuum. Thus,

[1]This can be appreciated from the Avogadro's number which specifies that at normal temperature and pressure, a gas will contain 6.022×10^{26} molecules per kmol. Thus in air, for example, there will be 10^{16} molecules per mm^3.

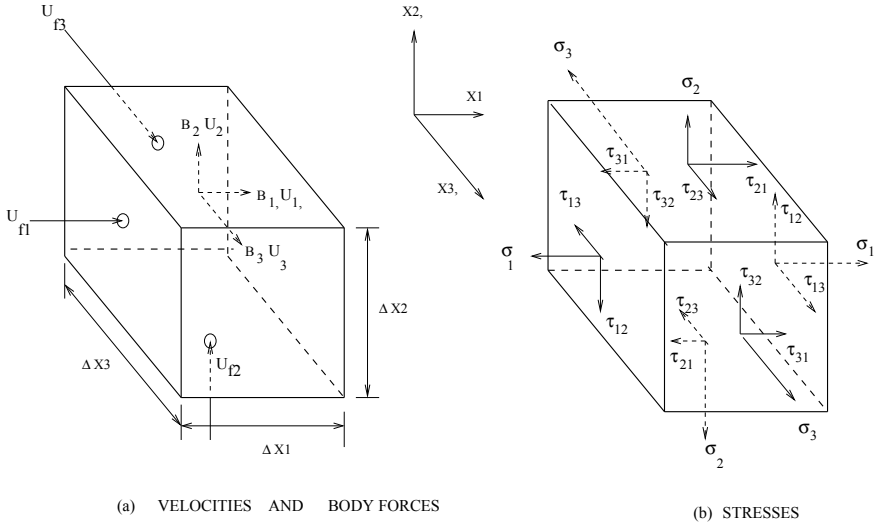

(a) VELOCITIES AND BODY FORCES (b) STRESSES

Fig. 1 Eulerian specifications of the control volume (CV)

$$\frac{\partial(\rho_m)}{\partial t} + \frac{\partial(\rho_m\, u_{fj})}{\partial x_j} = 0 \tag{1}$$

$$\frac{\partial(\rho_m\, u_i)}{\partial t} + \frac{\partial}{\partial x_j}(\rho_m\, u_{fj}\, u_i) = \frac{\partial \sigma_{xi}}{\partial x_i} + \frac{\partial}{\partial x_j}\left\{\tau_{ij}\,(1-\delta_{ij})\right\} + \rho_m\, B_i \tag{2}$$

$$\tau_{ij} = \mu\left[\frac{\partial u_i}{\partial x_j} + \frac{\partial u_j}{\partial x_i}\right] \tag{3}$$

where ρ_m is fluid (or mixture) density, u_{fj} are CV face velocities, u_j are representative CV velocities and B_i are volumetric body forces such as Buoyancy or Centrifugal or Coriolis force. Equation 3 expresses Stokes's law connecting surface stress τ_{ij} to the co-planar strain rate via fluid property μ. Finally, σ_{xi} are *total surface-normal (tensile) stresses* and are modelled as [27]

$$\begin{aligned}\sigma_{x_i} &\equiv -\,p + \sigma'_{xi} = -\,(p-q) + \tau_{ii} = -\,(p-q) + 2\,\mu\,\frac{\partial u_i}{\partial x_i}\\ &= -\,(p-q) + 2\,\mu\ \bigtriangledown\ .\ \vec{V}_f\end{aligned} \tag{4}$$

where pressure p is compressive, normal stress τ_{ii} are tensile and σ' is called the deviatoric stress. The significance of the newly introduced quantity q in its definition requires further elaboration.

1.2 Stokes's Continuum Condition

In Date [6], a quantity $\overline{p}$ is defined[2] as

$$\overline{p} \equiv -\frac{1}{3}\left(\sigma_{x_1} + \sigma_{x_2} + \sigma_{x_3}\right) \tag{5}$$

Now, an often overlooked *requirement* of the Stokes's relations (with or without variable properties and *in the absence of relaxation processes at the molecular level* [27]) is that $\overline{p}$ must equal the point value of pressure p and the latter, in turn, must equal thermodynamic pressure p_{th}. Thus, using Eq. 4, it follows that

$$\overline{p} = p = p_{\text{th}} = (p - q) - \frac{2}{3}\mu \ \bigtriangledown \ . \ \vec{V}_f \tag{6}$$

Now, to obey the above equality, q must be appropriately chosen in continuum as well as in discretised space. We now consider the following three cases:

1. Case 1: ($\vec{V} = 0$) In this *hydrostatic case*,

$$\overline{p} = p - q \tag{7}$$

But in this case, p can only vary linearly with x_1, x_2, x_3 and, therefore, the point value of p exactly equals its space averaged value $\overline{p}$ in both continuum and discretised space and hence

$$q = q_{\text{cont}} = q_{\text{disc}} = 0 \quad \rightarrow \quad \text{exactly} \tag{8}$$

2. Case 2: ($\mu = 0$ or $\bigtriangledown \ . \ V_f = 0$)

Clearly when $\mu = 0$ (inviscid flow) or $\bigtriangledown \ . \ V_f = \partial u_{fi}/\partial x_i = 0$ (constant density incompressible flow) $p = \overline{p}$ (Eq. 6) in a continuum, and hence $q_{\text{cont}} = 0$ exactly.[3] But, in this case, since fluid motion is considered, p can vary arbitrarily with x_1, x_2, x_3 and, therefore, p may not equal $\overline{p}$ in a *discrete space*. To understand this matter, consider a case in which pressure varies arbitrarily in x_1 direction whereas its variation in x_2 and x_3 directions is constant or linear (as in a hydrostatic case). Such a variation is shown in Fig. 2. Now consider a point P. According to Stokes's requirement, p_P must equal $\overline{p}_P$ in a continuum. But, in a discretised space, the values of pressure are available at points E and W only, and if these points are

[2] In [27], symbol $\overline{\sigma} = (\sum_{i=1}^{3} \sigma_{xi})/3$ is used. Here, $\overline{p} = -\overline{\sigma}$ is preferred. Both $\overline{p}$ and q are newly introduced to serve a pedagogic purpose.

[3] It is important to recognise that in discretised CFD, the incompressible condition ($\bigtriangledown \ . \ V_f = 0$) is defined in terms of CV face velocities u_{fi} as shown in Fig. 1. In fact, when this definition is explicitly implemented, there results the SIMPLE staggered grid procedure of Patankar and Spalding [19]. Further, u_{fi} must *satisfy momentum equations*. In a continuum, u_{fi} and u_i fields coincide but in a discretised space, it is important to distinguish them. This will become apparent in the next section.

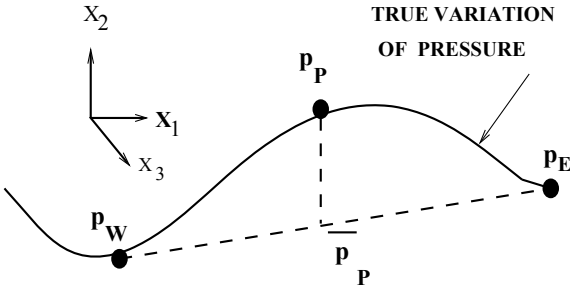

Fig. 2 1D variation of pressure and Stokes's requirement

equi-distant from P then $\overline{p}_P = 0.5\,(p_W + p_E)$. Now, this $\overline{p}_P$ *will not equal* p_P as seen from the figure and, therefore, the requirement of the Stokes's relations is not met.

However, without violating the continuum requirement, we may set

$$q = q_{\text{cont}} = q_{\text{disc}} = \lambda\,(p - \overline{p}) \tag{9}$$

where λ is an arbitrary constant. In most textbooks, where continuum is assumed, λ is trivially set to zero because $p = \overline{p}$ (Eq. 6) in a continuum.

3. Case 3: ($\mu \neq 0$ or $\bigtriangledown \,.\, V_f \neq 0$)

This case represents either compressible flow where density is a state function of both temperature and pressure or an incompressible flow with density dependent on temperature or any other scalar (e.g. void or volume fraction). Thus, in this case, Stokes's requirement will be satisfied (see Eq. 6) if we set

$$q = \lambda\,(p - \overline{p}) + \gamma\ \bigtriangledown\ .\, V_f \qquad \rightarrow \qquad \gamma = -\frac{2}{3}\,\mu \tag{10}$$

where γ is the well-known second viscosity coefficient whose value is routinely set to $-(2/3)\mu$ *even in a continuum*. It is instructive to note the reason for this setting. Because, if this was not done then by combining Eqs. 10 and 6, it can be shown that

$$(1 - \lambda)\,(p - \overline{p})\ \bigtriangledown\ .\, V_f = \left(\gamma + \frac{2}{3}\,\mu\right)\,(\bigtriangledown\,.\,V_f)^2 \tag{11}$$

Clearly, this equation suggests that the system will experience *dissipation* (or reversible work done at finite rate since $\bigtriangledown\,.\,V_f$ is associated with the *rate of volume change*) even in an *isothermal flow* [27, 36]. This is, of course, highly improbable.[4]

[4]In passing we note that in all three cases, it can be verified that the quantity q is invariant under rotation of the coordinate system or interchange of axes. This property ensures isotropy [27].

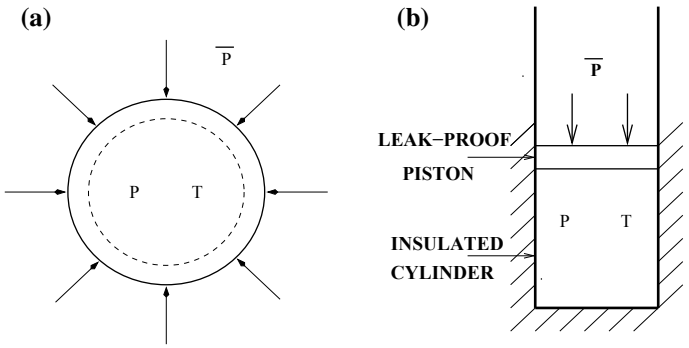

Fig. 3 Consequences of violating Stokes's condition **a** isolated spherical mass of fluid [27], **b** insulated piston cylinder

1.3 Thermodynamic Explanations

This improbability has been explained by Schlichting [27] by considering the case of an isolated spherical mass of *isothermal fluid* subjected to uniform normal stress $\overline{\sigma} = -\overline{p}$ (see Fig. 3a). Now, if γ is not set to $-(2/3)\mu$, the sphere will undergo radial oscillations of compression and expansion. Here, however, we consider an alternative arrangement that will yield one further interpretation.

Figure 3b shows the piston-cylinder arrangement typically used in undergraduate thermodynamics. The system fluid is held in a leakproof adiabatic cylinder at temperature T and pressure p. The system is in equilibrium. Now, suppose the unlikely circumstance in which external pressure $\overline{p}$ exceeds system pressure p. It is obvious that the piston will move downwards compressing the fluid. But, if we now require that the temperature of the fluid must remain constant at T (this is analogous the Schlichting's isothermal flow), then clearly, from first law of thermodynamics, no change in internal energy ΔU is permitted in an adiabatic cylinder, and hence there can only be two consequences.

1. The piston will instantly *bounce back* to its original position to restore equilibrium. The process may repeat resulting in oscillations of the piston *in time*. However, in a *steady-state* problem, these oscillations will manifest as *spatially zig-zag* pressure.
2. Alternatively, to maintain constant internal energy, some fluid must *somehow leak out* although the piston is leakproof.

It is obvious that both these occurrences are improbable but are nonetheless encountered in discretised CFD when Stokes's continuum condition (6) is violated as will be shown in Sects. 2 and 3. Incidentally, the second circumstance above is a new interpretation associated with the violation of the Stokes's condition.

Thus, as shown in Eq. 10, the Stokes's relations for normal stress require modifications *even in a continuum* when compressible flow is considered (requiring introduction of the so-called second viscosity coefficient) and a physical explanation for this modification is found from Thermodynamics. Now, the same interpretation can be afforded to $\lambda\,(p-\overline{p})$ part of q in Eqs. 9 or 10. This term represents a necessary modification in a discretised space. This is an important departure from the forms of normal stress expressions given in standard textbooks on fluid mechanics.

1.4 Appropriate Forms of N-S Equations

Finally, from the above discussion, it is clear that the Navier–Stokes equations written out for finite-volume discretisation should preferably read as

$$\frac{\partial(\rho_m)}{\partial t}+\frac{\partial(\rho_m\,u_{fj})}{\partial x_j}=0 \tag{12}$$

$$\frac{\partial(\rho_m\,u_i)}{\partial t}+\frac{\partial}{\partial x_j}(\rho_m\,u_{fj}\,u_i)=-\frac{\partial(p-q)}{\partial x_i}+\frac{\partial}{\partial x_j}\left\{\tau_{ij}\right\}+\rho_m\,B_i \tag{13}$$

where, in the most general case, q stands for

$$q=\lambda\,(p-\overline{p})-\frac{2}{3}\,\mu\times\nabla\,.\,\vec{V}_f \tag{14}$$

Of course, $\lambda=0$ in a continuum but finite[5] in a discretised space. Note, however, that in the latter, as mesh size is reduced, $p\to\overline{p}$, and hence $q_{\text{disc}}\to q_{\text{cont}}$. Also, it is important to note that since $\overline{p}$ must equal point value of pressure p in a continuum (see Eq. 6), the former must essentially correspond to the *hydrostatic or spatially linear* variation of pressure (in a local sense) irrespective of the flow considered. Mathematically, therefore, we may define $\overline{p}$ as

$$\overline{p}=-\frac{1}{3}\sum_{i=1}^{3}\sigma_{x_i}=\frac{1}{3}\sum_{i=1}^{3}\overline{p}_{x_i} \tag{15}$$

where $\overline{p}_{x_i}$ are each a solution[6] to

$$\frac{\partial^2 p}{\partial x_i^2}=0 \tag{16}$$

This manner of evaluation of $\overline{p}$ can be implemented on both structured and unstructured meshes [4–7, 22, 23] in discretised CFD.

[5] Analysis of the discretised equations presented in the next section shows that $\lambda=0.5$.

[6] Equation 16 is validated in Eqs. 39–43 for a two-dimensional flow.

2 Computations on Colocated Grids

2.1 Pressure-Correction Equation on Colocated Grids

Since it has been known that in the SIMPLE algorithm [19], zig-zag pressure prediction is avoided by the use of staggered grid arrangement of pressure and the velocity variables (see Fig. 4a), it is obvious that the pressure-correction equation applicable to colocated grids must mimic the main features of the staggered grid practice. Thus, we begin by stating that in a fully implicit iterative procedure, the cell-face velocity will be calculated from

$$u_{fi}^{l+1} = \frac{\alpha}{AP^{u_{fi}}} \left[\sum_k A_k u_{fi,k}^{l+1} - \Delta V \frac{\partial p^{l+1}}{\partial x_i} \right] + (1-\alpha)\, u_{fi}^{l} \tag{17}$$

where $AP^{u_{fi}} = \sum A_k + \rho_m^0 \, \Delta V / \Delta t$. Now, this velocity field must satisfy mass conservation equation (1). Thus

$$\frac{\partial(\rho_m^{l+1})}{\partial t} + \frac{\partial(\rho_m^{l+1}\, u_{fi}^{l+1})}{\partial x_i} = 0 \tag{18}$$

After substituting Eq. 17 in Eq. 18, we make use of following representations:

$$u_{fi}^{l+1} = u_{fi}^{l} + u_{fi}^{'} \qquad \text{and} \qquad p^{l+1} = p^{l} + p_m^{'} \tag{19}$$

The above operations result[7] in

$$\frac{\partial}{\partial x_i}\left[\rho_m^{l+1}\, D_i \frac{\partial p_m^{'}}{\partial x_i}\right] = \frac{\partial(\rho_m^{l+1})}{\partial t} + \frac{\partial(\rho_m^{l+1}\, u_{fi}^{l})}{\partial x_i} - \frac{\partial}{\partial x_i}\left[\rho_m^{l+1}\, D_i\, R_{ufi}\right] \quad \rightarrow D_i = \frac{\alpha\, \Delta V}{A p^{u_{fi}}} \tag{20}$$

where R_{ufi} is the residual per unit volume and is given by

$$R_{ufi} = \frac{AP^{ufi}\, u_{fi}^{l} - \sum A_k u_{fi,k}^{l}}{\Delta V} + \frac{\partial p^{l}}{\partial x_i} \tag{21}$$

[7] In deriving Eq. 20, it is assumed that $\sum A_k\, u_{fi,k}^{'} = 0$. This is consistent with the staggered grid practice [19].

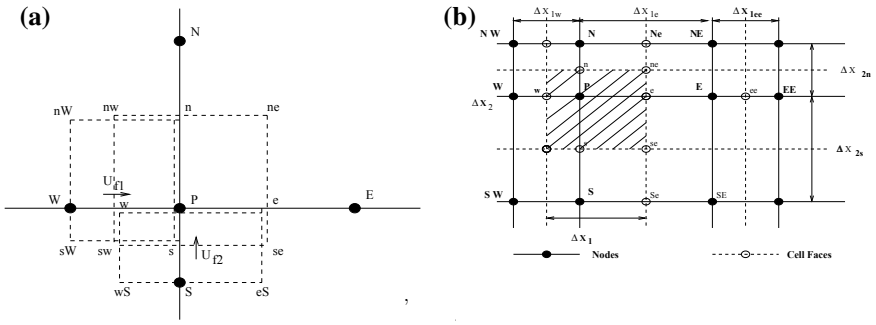

Fig. 4 **a** Staggered grid arrangement of variables and associated CVs, **b** colocated grids—cell faces are midway between the adjacent nodes

2.2 Analysis of Discretised Equation

To understand further developments of this paper, following comments are now pertinent:

1. On both staggered and colocated grids, the pressure is stored at node P and the mass conservation equation is solved over the control volume surrounding node P. Therefore, with reference to Fig. 4b, the discretised version of Eq. 20 in two dimensions will read as

$$AP\ p'_{m,P} = AE\ p'_{m,E} + AW\ p'_{m,W} + AN\ p'_{m,N} + AS\ p'_{m,S} - \dot{m}_P + \dot{m}_R \tag{22}$$

where

$$\begin{aligned} AE &= \frac{\rho_m^{l+1}\ \alpha\ \Delta x_2^2}{AP^{uf1}}\,|_e, \quad AW = \frac{\rho_m^{l+1}\ \alpha\ \Delta x_2^2}{AP^{uf1}}\,|_w \\ AN &= \frac{\rho_m^{l+1}\ \alpha\ \Delta x_1^2}{AP^{uf2}}\,|_n, \quad AS = \frac{\rho_m^{l+1}\ \alpha\ \Delta x_1^2}{AP^{uf2}}\,|_s \\ AP &= AE + AW + AN + AS \end{aligned} \tag{23}$$

Further, the mass source $\dot{m}_P$ and residual source $\dot{m}_R$ will be given by

$$\begin{aligned} \dot{m}_P &= (\rho_m^{l+1}\ u_{f1}^l\,|_e - \rho_m^{l+1}\ u_{f1}^l\,|_w)\ \Delta x_2 \\ &\quad + (\rho_m^{l+1}\ u_{f2}^l\,|_n - \rho_m^{l+1}\ u_{f2}^l\,|_s)\ \Delta x_1 \\ &\quad + (\rho_{m,P}^{l+1} - \rho_{m,P}^{o})\ \frac{\Delta V}{\Delta t} \end{aligned} \tag{24}$$

$$\begin{aligned} \dot{m}_R &= AE\ R_{uf1}\ \Delta x_1|_e - AW\ R_{uf1}\ \Delta x_1|_w \\ &\quad + AN\ R_{uf2}\ \Delta x_2|_n - AS\ R_{uf2}\ \Delta x_2|_s \end{aligned} \tag{25}$$

2. On staggered grids, momentum equations are solved at the cell faces and, therefore, residuals R_{uf1} and R_{uf2} must vanish at full convergence rendering $\dot{m}_R = 0$. Although this state of affairs will prevail only at convergence, one may ignore $\dot{m}_R$ *even during iterative solution*. Thus, effectively, Eq. 20 applicable to staggered grid arrangement is

$$\frac{\partial}{\partial x_i}\left[\rho_m^{l+1}\, D_i\, \frac{\partial p_m^{'}}{\partial x_i}\right] = \frac{\partial(\rho_m^{l+1})}{\partial t} + \frac{\partial(\rho_m^{l+1}\, u_{fi}^{l})}{\partial x_i} \tag{26}$$

The above equation is solved with the boundary condition [19]

$$\frac{\partial p_m^{'}}{\partial n}\,|_b = 0 \tag{27}$$

If the boundary pressure p_b is specified then, of course, $p_{m,b}^{'} = 0$.

3. When computing on colocated grid, however, cell-face velocities must be evaluated by interpolation to complete evaluation of $\dot{m}_P$ because only nodal velocities $u_{i,P}$ are computed through momentum equations. Thus, $\dot{m}_P$ in Eq. 24 is evaluated as

$$\begin{aligned}\overline{\dot{m}}_P &= (\rho_m^{l+1}\,\overline{u}_1^{l}\,|_e - \rho_m^{l+1}\,\overline{u}_1^{l}\,|_w)\,\Delta x_2 \\ &+ (\rho_m^{l+1}\,\overline{u}_2^{l}\,|_n - \rho_m^{l+1}\,\overline{u}_2^{l}\,|_s)\,\Delta x_1 \\ &+ (\,\rho_{m,P}^{l+1} - \rho_{m,P}^{o}\,)\,\frac{\Delta V}{\Delta t}\end{aligned} \tag{28}$$

where the mean velocities $\overline{u}_i$ are evaluated by one-dimensional averaging although multidimensional averaging can also be preferred. Thus, since the cell faces are midway between the nodes, we may write

$$\begin{aligned}\overline{u}_{1,e} &= \frac{1}{2}\,(u_{1,P} + u_{1,E}) \qquad & \overline{u}_{1,w} &= \frac{1}{2}\,(u_{1,P} + u_{1,W}) \\ \overline{u}_{2,n} &= \frac{1}{2}\,(u_{2,P} + u_{2,N}) \qquad & \overline{u}_{2,s} &= \frac{1}{2}\,(u_{2,P} + u_{2,S})\end{aligned} \tag{29}$$

Replacing $u_{f1,e}$ by $\overline{u}_{1,e}$, etc. in the above manner, of course, does not guarantee that $\dot{m}_P$ will vanish *even at convergence.*[8]

4. Similarly, to evaluate $\dot{m}_R$ from Eq. 25, we reconsider Eq. 21 for cell-face location e, for example, and write it as

$$R_{u_{f1,e}} = \overline{\frac{A P^{u_{f1}} u^l_{f1} - \sum A_k u^l_{f1,k}}{\Delta V}} \mid_e + \frac{\partial p^l}{\partial x_1} \mid_e \tag{33}$$

In this equation, the net-momentum-transfer terms are now *multidimensionally averaged*. This is necessary because when computing on colocated grids, coefficients A_k are not available at the cell-face locations. Thus, again using Eq. 21, we have

$$\overline{\frac{A P^{u_{f1}} u^l_{f1} - \sum A_k u^l_{f1,k}}{\Delta V}} \mid_e = \overline{R}_{u_{f1,e}} - \overline{\frac{\partial p^l}{\partial x_1}} \mid_e \tag{34}$$

Effectively, therefore

$$R_{u_{f1,e}} = \overline{R}_{u_{f1,e}} - \overline{\frac{\partial p^l}{\partial x_1}} \mid_e + \frac{\partial p^l}{\partial x_1} \mid_e \tag{35}$$

5. Multidimensionally averaged $\overline{R}_{u_{f1,e}}$ is evaluated as

---

[8] Incidentally, in the literature, several different types of interpolations have been proposed. Some of these are given below by way of example.

- Rhie and Chow [24] (1D Pressure gradient interpolation)

$$u_{f1,e} = \overline{u}_{1,e} - \frac{\Delta V}{A P^u} \left[\frac{\partial p}{\partial x_1} \mid_e - \overline{\frac{\partial p}{\partial x_1}} \mid_e \right]$$
$$\text{where} \quad \overline{\frac{\partial p}{\partial x_1}} \mid_e = \frac{1}{2} \left[\frac{\partial p}{\partial x_1} \mid_P + \frac{\partial p}{\partial x_1} \mid_E \right] \tag{30}$$

- Peric [8] (1D Mom-Outflow interpolation)

$$u_{f1,e} = \frac{1}{2} \left[\frac{\sum A_k u_{1,k}}{A P^{u_1}} \mid_P + \frac{\sum A_k u_{1,k}}{A P^{u_1}} \mid_E \right] - \frac{\Delta V}{A P^u} \frac{\partial p}{\partial x_1} \mid_e \tag{31}$$

- Thiart [34] (Power Law Scheme [20])

$$\begin{aligned} u_{f1,e} &= \theta\, u_{1,P} + (1-\theta)\, u_{1,E} \qquad \text{where} \\ \theta(Pc_e) &= [Pc_e - 1 + \max(0, -Pc_e)] / Pc_e \\ &\quad + \max\left\{0, (1 - 0.1|Pc_e|)^5\right\} / Pc_e \end{aligned} \tag{32}$$

where cell-face Reynolds/Peclet number $Pc_e = (\rho_m\, u_{f1} \Delta x_1 / \mu)_e$.

$$\overline{R}_{u_{f1,e}} = \frac{1}{2}\left[\frac{1}{2}\left(R_{u1,P} + R_{u1,E}\right) + \frac{\Delta x_{2,n}\, R_{u1,se} + \Delta x_{2,s}\, R_{u1,ne}}{\Delta x_{2,n} + \Delta x_{2,s}}\right]$$
$$R_{u1,se} = \frac{1}{4}\left(R_{u1,P} + R_{u1,E} + R_{u1,S} + R_{u1,SE}\right)$$
$$R_{u1,ne} = \frac{1}{4}\left(R_{u1,P} + R_{u1,E} + R_{u1,N} + R_{u1,NE}\right) \tag{36}$$

This representation shows that effectively residuals at nodal locations *P*, *E*, *N*, *S*, *NE* and *SE* only are involved. These residuals will, of course, vanish at full convergence because momentum equations are being solved at the nodal positions. Therefore, effectively $\overline{R}_{u_{f1,e}} = 0$ at convergence and Eq. 35 can be written as

$$R_{u_{f1,e}} = \frac{\partial p^l}{\partial x_1}\,|_e - \overline{\frac{\partial p^l}{\partial x_1}}\,|_e \tag{37}$$

6. Now, to evaluate multidimensionally averaged pressure gradient in the above equation, we write

$$\begin{aligned}\overline{\frac{\partial p^l}{\partial x_1}}\,|_e &= \frac{1}{2}\left[\frac{1}{2}\left(\frac{\partial p^l}{\partial x_1}\,|_P + \frac{\partial p^l}{\partial x_1}\,|_E\right)\right.\\ &\quad\left. + \frac{\Delta x_{2,n}\,\partial p^l/\partial x_1\,|_{se} + \Delta x_{2,s}\,\partial p^l/\partial x_1\,|_{ne}}{\Delta x_{2,n} + \Delta x_{2,s}}\right]\\ &= \frac{1}{4}\left[\frac{p^l_E - p^l_W}{\Delta x_{1,e} + \Delta x_{1,w}} + \frac{p^l_{EE} - p^l_P}{\Delta x_{1,e} + \Delta x_{1,w}}\right]\\ &\quad + \frac{1}{4}\,\frac{\Delta x_{2,s}}{\Delta x_{2,n} + \Delta x_{2,s}}\left[\frac{p^l_E + p^l_{NE} - p^l_P - p^l_N}{\Delta x_{1,e}}\right]\\ &\quad + \frac{1}{4}\,\frac{\Delta x_{2,n}}{\Delta x_{2,n} + \Delta x_{2,s}}\left[\frac{p^l_E + p^l_{SE} - p^l_P - p^l_S}{\Delta x_{1,e}}\right]\end{aligned} \tag{38}$$

To simplify the above evaluation further, following definitions are introduced allowing for the non-uniform grid spacing:

$$\overline{p^l}_{x_1,P} \equiv \frac{\Delta x_{1,w}\, p^l_E + \Delta x_{1,e}\, p^l_W}{\Delta x_{1,w} + \Delta x_{1,e}} \qquad \left(\text{solution to } \frac{\partial^2 p^l}{\partial x_1^2}|_P = 0\right) \tag{39}$$
$$\overline{p^l}_{x_2,P} \equiv \frac{\Delta x_{2,s}\, p^l_N + \Delta x_{2,n}\, p^l_S}{\Delta x_{2,s} + \Delta x_{2,n}} \qquad \left(\text{solution to } \frac{\partial^2 p^l}{\partial x_2^2}|_P = 0\right) \tag{40}$$
$$\overline{p^l}_P = \frac{1}{2}\left(\overline{p^l}_{x_1,P} + \overline{p^l}_{x_2,P}\right) \tag{41}$$

$$\overline{p^l}_{x_1,E} \equiv \frac{\Delta x_{1,e}\, p^l_{EE} + \Delta x_{1,ee}\, p^l_P}{\Delta x_{1,e} + \Delta x_{1,ee}} \qquad \text{(solution to } \frac{\partial^2 p^l}{\partial x_1^2}|_E = 0) \tag{42}$$

$$\overline{p^l}_{x_2,E} \equiv \frac{\Delta x_{2,s}\, p^l_{NE} + \Delta x_{2,n}\, p^l_{SE}}{\Delta x_{2,s} + \Delta x_{2,n}} \qquad \text{(solution to } \frac{\partial^2 p^l}{\partial x_2^2}|_E = 0) \tag{43}$$

$$\overline{p^l}_E = \frac{1}{2}\,(\overline{p^l}_{x_1,E} + \overline{p^l}_{x_2,E}) \tag{44}$$

Substituting the above definitions[9] in Eq. 38 and replacing p^l_{EE} (Eq. 42) and p^l_W (Eq. 39), respectively, in favour of p^l_E and p^l_P, it can be shown that

$$\begin{aligned}\overline{\frac{\partial p^l}{\partial x_1}}\,|_e &= \frac{1}{2}\left[\frac{p^l_E - p^l_P}{\Delta x_{1,e}} + \frac{\overline{p}^l_E - \overline{p}^l_P}{\Delta x_{1,e}}\right] \\ &= \frac{1}{2}\,\frac{\partial(\,p^l + \overline{p}^l\,)}{\partial x_1}\,|_e\end{aligned} \tag{45}$$

and, therefore, from Eq. 37

$$R_{u_{f1,e}} = \frac{\partial p^l}{\partial x_1}\,|_e - \frac{1}{2}\,\frac{\partial(\,p^l + \overline{p}^l\,)}{\partial x_1}\,|_e = \frac{1}{2}\,\frac{\partial(p^l - \overline{p}^l)}{\partial x_1}\,|_e = \frac{\partial p^{'}_{sm}}{\partial x_1}\,|_e \tag{46}$$

where

$$p^{'}_{sm} = \frac{1}{2}\,(p^l - \overline{p}^l) \qquad \text{(Smoothing Pressure Correction)} \tag{47}$$

Note that the analysis of the discretised equations has yielded a value $\lambda = 0.5$ and $q = p^{'}_{sm}$ (see Eq. 9).

7. Repeating items 4, 5 and 6 at other cell faces, it can be shown that

$$R_{u_{f1,w,e}} = \frac{\partial p^{'}_{sm}}{\partial x_1}\,|_{w,e} \qquad R_{u_{f2,s,n}} = \frac{\partial p^{'}_{sm}}{\partial x_2}\,|_{s,n} \tag{48}$$

Thus, substituting the above equations in Eq. 25, it follows that

$$\begin{aligned}\dot{m}_R = {} & AE\,\frac{\partial p^{'}_{sm}}{\partial x_1}\,\Delta x_1|_e - AW\,\frac{\partial p^{'}_{sm}}{\partial x_1}\,\Delta x_1|_w \\ & + AN\,\frac{\partial p^{'}_{sm}}{\partial x_2}\,\Delta x_2|_n - AS\,\frac{\partial p^{'}_{sm}}{\partial x_2}\,\Delta x_2|_s\end{aligned} \tag{49}$$

8. In evaluating coefficients AE, AW, AN and AS, we need AP coefficients at the cell faces (see Eq. 23). But, these can be evaluated by one-dimensional averaging as

[9] Equations 39–43 justify the assertion made in Eqs. 15 and 16 for a two-dimensional flow.

$$AP_e^{uf1} = \frac{1}{2}(AP_P^{u_1} + AP_E^{u_1}) \qquad AP_w^{uf1} = \frac{1}{2}(AP_P^{u_1} + AP_W^{u_1})$$
$$AP_n^{uf2} = \frac{1}{2}(AP_P^{u_2} + AP_N^{u_2}) \qquad AP_s^{uf2} = \frac{1}{2}(AP_P^{u_2} + AP_S^{u_2}) \tag{50}$$

where the AP coefficients at the nodal locations P, N, E, S, W are known on colocated grids.

9. The above derivations show that Eqs. 24 and 25 can be replaced by Eqs. 28 and 49, respectively. Thus, the mass-conserving pressure-correction Eq. 20 appropriate for colocated grids can effectively be written as

$$\frac{\partial}{\partial x_i}\left[\rho_m^{l+1}\, D_i\, \frac{\partial p_m^{'}}{\partial x_i}\right] = \frac{\partial(\rho_m^{l+1})}{\partial t} + \frac{\partial(\rho_m^{l+1}\, \overline{u}_i^{l})}{\partial x_i} - \frac{\partial}{\partial x_i}\left[\rho_m^{l+1}\, D_i\, \frac{\partial p_{sm}^{'}}{\partial x_i}\right] \tag{51}$$

2.2.1 Further Simplification

It is possible to further simplify Eq. 51. To understand this simplification, consider, for example, the grid disposition near the west boundary as shown in Fig. 5. When computing at the near-boundary node $P(2,j)$, the pressure gradient $\partial p/\partial x_1\,|_P$ must be evaluated in the momentum equation for velocity $u_{1,P}$. This will require knowledge of boundary pressure $p_b = p\,(1,\, j)$. On colocated grids, this pressure is not known and, therefore, is evaluated by *linear* extrapolation from interior flow points. Thus,

$$p_b = \frac{L_{bE}}{L_{PE}}\, p_P - \frac{L_{bP}}{L_{PE}}\, p_E \tag{52}$$

where L denotes length. The same procedure is adopted at Nb and Sb. Now, assuming that the pressure variation near a boundary is *locally* linear in both x_1 and x_2 directions, it follows that

$$p_b - \overline{p}_b = p_P - \overline{p}_P \qquad \text{or} \qquad p_{sm,b}^{'} = p_{sm,P}^{'} \tag{53}$$

and, therefore,

$$\frac{\partial p_{sm}^{'}}{\partial x_1}\,|_b = \frac{\partial p_{sm}^{'}}{\partial n}\,|_b = 0 \tag{54}$$

The same condition is also applicable to $p_m^{'}$ (see Eq. 27). Now, Eq. 51 shows that multipliers of gradients of $p_m^{'}$ and $p_{sm}^{'}$ are identical and since the boundary conditions for these two variables are also identical, we may write the mass-conserving pressure correction in the following form:

$$\frac{\partial}{\partial x_i}\left[\rho_m^{l+1}\, D_i\, \frac{\partial p^{'}}{\partial x_i}\right] = \frac{\partial(\rho_m^{l+1})}{\partial t} + \frac{\partial(\rho_m^{l+1}\, \overline{u}_i^{l})}{\partial x_i} \tag{55}$$

where $p^{'}$ is called *total pressure correction* and is expressed as

$$p^{'} = p_m^{'} + p_{sm}^{'} \tag{56}$$

Here, $p_{sm}^{'}$, of course, is evaluated from Eq. 47. Following Eqs. 54 and 27, Eq. 55 must be solved with boundary condition

$$\frac{\partial p^{'}}{\partial x_1}\,|_b = \frac{\partial p^{'}}{\partial n}\,|_b = 0 \tag{57}$$

The discretised form of Eq. 55 is

$$AP\; p_P^{'} = AE\; p_E^{'} + AW\; p_W^{'} + AN\; p_N^{'} + AS\; p_s^{'} - \overline{\dot{m}}_P \tag{58}$$

where $\overline{\dot{m}}_P$ is given by Eq. 28.

Finally, note that Eq. 55 has similarity with the staggered grid equation (26). Both are Poisson's equations with similar boundary conditions (57) and (27).

2.2.2 Modification for Compressible Flow

So far it has been assumed that ρ_m = constant as in incompressible flow. However, in compressible flow ρ_m is connected to pressure p via equation of state such as $p = \rho_m\, R_g\, T$. Thus,

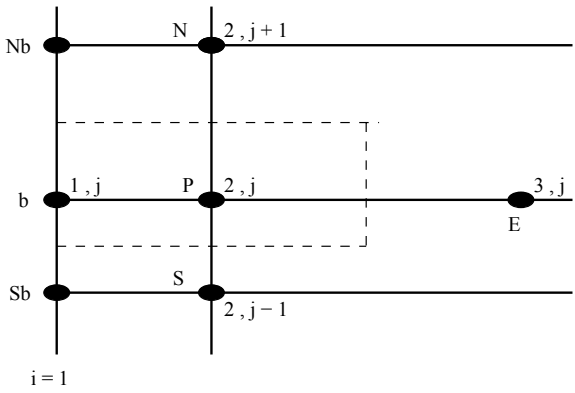

Fig. 5 West boundary $I = 1$

$$\rho_m^{l+1} = \rho_m^l + \rho_m^{'} = \rho_m^l + \frac{p_m^{'}}{R_g\, T} = \rho_m^l + \frac{p^{'} - p_{sm}^{'}}{R_g\, T} \tag{59}$$

With this substitution, Eq. 55 will read as

$$\frac{\partial}{\partial x_i}\left[\rho_m^l\, D_i\, \frac{\partial p^{'}}{\partial x_i} - U_i^*\, \frac{p^{'}}{R_g T}\right] = \frac{\partial(\rho_m^l)}{\partial t} + \frac{\partial}{\partial x_i}\left[\rho_m^l\, \overline{u}_i^l - U_i^*\, \frac{p_{sm}^{'}}{R_g T}\right] \tag{60}$$

$$U_i^* = u_i^l - D_i\, \frac{\partial p_{sm}^{'}}{\partial x_i} \tag{61}$$

The left-hand side of Eq. 60 contains diffusion ($D_i \partial p^{'}/\partial x_i$) as well as convection ($U_i^*\, p^{'}/R_g T$) terms. Thus, for compressible flow, the pressure-correction equation is a transport equation for $p^{'}$ and not a Poisson's equation. Also, note that if $U_i^* = 0$, the incompressible form (see Eq. 51) is recovered.

2.2.3 Overall Calculation Procedure on Colocated Grids

The sequence of calculations on colocated grids is as follows:

1. At a given time step, guess pressure field p^l. This may be the pressure field from the previous time step.
2. Solve momentum equations once for each u_i with problem-dependent boundary conditions. Thus

$$AP^{u_i}\, u_{i,P}^l = \sum A_k^{u_i}\, u_{i,k}^l - \Delta V\, \frac{\partial p^l}{\partial x_i}|_P + \frac{\rho_{m,p}^o\, \Delta V}{\Delta t}\, u_{i,P}^o \tag{62}$$

   where $AP^{u_i} = \sum A_k^{u_i} + \rho_m^0\, \Delta V/\Delta t$.
3. Using the u_i^l distribution, solve Eq. 55 (or, 60) with boundary condition (57) to yield the total pressure correction $p_{i,j}^{'}$ field. This implies iterative solution of Eq. 58. The number of iterations typically may not exceed 10.
4. Recover mass-conserving pressure correction via Eq. 56. Thus

$$p_{m,P}^{'} = p_P^{'} - p_{sm,P}^{'} = p_P^{'} - \frac{1}{2}\,(p_P^l - \overline{p}_P^l) \tag{63}$$

   where $\overline{p}_P^l$ is evaluated from Eqs. 15 and 16. Using this $p_m^{'}$ field, the mass conservation error is evaluated from[10]

$$R_{\text{mass},P} = AP\; p_{m,P}^{'} - (AE p_{m,E}^{'} + AW p_{m,W}^{'} + AN p_{m,N}^{'} + AS p_{m,S}^{'}) \tag{64}$$

[10]This is unlike the staggered grid practice in which the mass error is estimated from discretised version of Eq. 1.

5. Correct pressure and velocity fields according to

$$p_P^{l+1} = p_P^l + \beta\, p'_{m,P} \qquad \text{where} \qquad 0 < \beta < 1 \tag{65}$$

$$u_{i,P}^{l+1} = u_{i,P}^l - D_i \frac{\partial p'_m}{\partial x_i}|_P \tag{66}$$

6. Using this new velocity field, solve discretised forms of scalar transport equations relevant to the problem at hand.
7. Evaluate residuals R_Φ of momentum and scalar (Φ) equations. The mass residual R_m evaluated from Eq. 64. When maximum residual as per the L2-norm is $<10^{-5}$, convergence is declared.
8. If this convergence criterion is not satisfied, treat $p^{l+1} = p^l, u_i^{l+1} = u_i^l$ and $\Phi^{l+1} = \Phi^l$ and return to step 2.
9. To execute the next time step, set $u_i^o = u_i^{l+1}$, $\Phi^o = \Phi^{l+1}$ and return to step 1.

2.3 *Some Illustrative Problems*

In all problems, computations are carried out with ($\lambda = 0.5$) and without ($\lambda = 0$) application of smoothing pressure correction.

2.3.1 Essentially Parabolic Flows

We consider 2D laminar developing flow between two parallel plates $2b$ apart ($D_h = 4b$). Although the flow is parabolic, here it is treated as being governed by 2D elliptic equations.

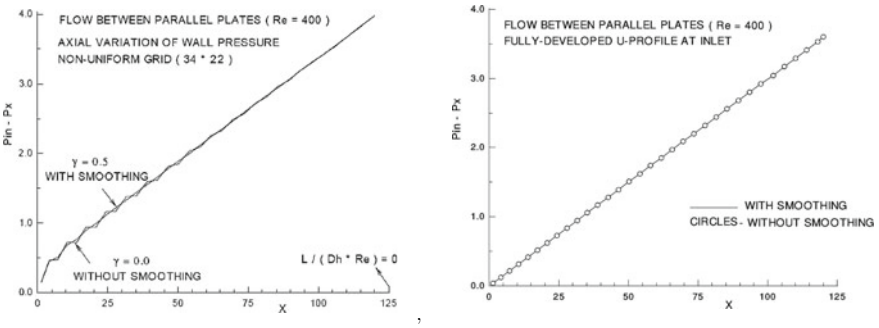

(a) $u_{in} = \overline{u}$, (b) $\frac{u_{in}}{\overline{u}} = \frac{3}{2}\left\{1 - (\frac{y}{b})^2\right\}$

Fig. 6 Entrance region flow between parallel plates

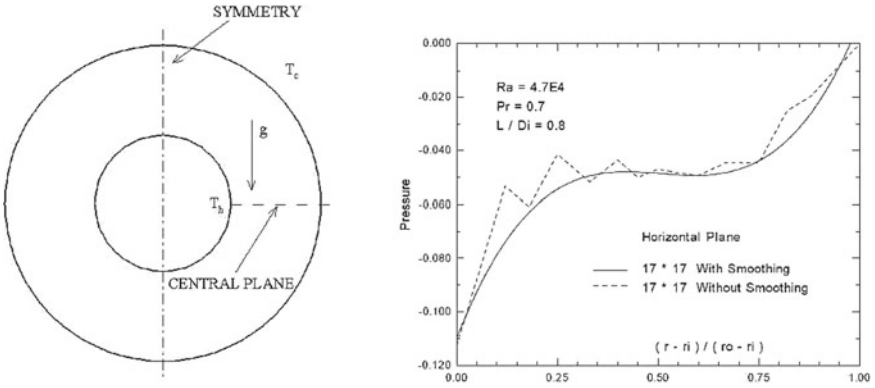

Fig. 7 Natural convection in horizontal concentric annulus [4]

Figure 6a shows predicted axial variation of wall pressure for the case when the fluid enters the channel with uniform axial velocity $u_{\text{in}} = \overline{u}$. As the boundary layers develop along the channel walls, the true pressure variation is expected to be non-linear with x in the entrance region but, at large x, it is expected to be linear because the flow is now fully developed. It is seen that with $\lambda = 0$, the predicted pressure is zig-zag near the entrance, whereas at large x, pressure zig-zagness disappears.

In contrast, Fig. 6b shows predictions for the case in which the fluid enters with fully developed parabolic axial velocity profile. Then, it is expected that true axial pressure variation will be linear right from the $x = 0$. Figure 6b confirms this expectation even when $\lambda = 0$.

2.3.2 Essentially Elliptic Flows

Natural Convection: Figure 7 (left) shows concentric cylinders in which the inner cylinder (dia D_i) is hotter (T_h) than the outer (T_c) one (dia D_o). The annulus gap width $L = (D_o - D_i)/2$. Figure 7 (right) shows predicted pressure variation along the horizontal plane in the presence of natural convection. Here again, since the true pressure variation is non-linear, the predicted pressure with $\lambda = 0$ shows zig-zagness. But, with smoothing pressure correction ($\lambda = 0.5$), zig-zagness disappears. The annulus natural convection flow is fully elliptic that involves simultaneous solution of the energy equation along with the flow equations. Further, the domain of computation is mapped by unstructured grid of triangular elements [4].

Mixed Convection: We now consider the problem of mixed convection flow in a right-angled corner. As shown in Fig. 8 (top), flow enters the domain of computation at the north boundary, turns anticlockwise around the corner and leaves through the east boundary. For this problem, an exact solution is developed by Shih and Ren [28] by specifying *artificial boundary conditions*. The unique feature of the exact solution is that the pressure variation in Y-direction is linear at all constant X-planes.

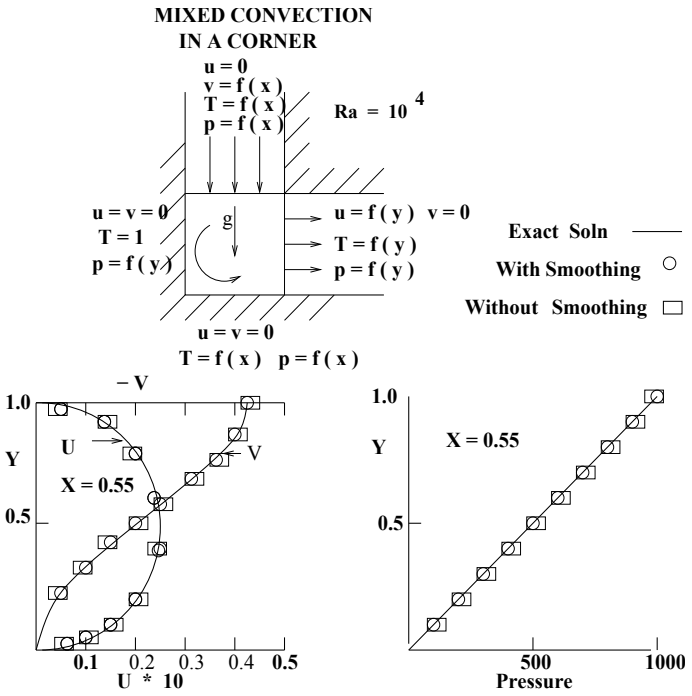

Fig. 8 Mixed convection in a corner—artificial boundary conditions

Figure 8 (left) shows comparison of predicted and exact profiles of velocity (u and v). Similar comparison for pressure is shown in Fig. 8 (right). It is seen that since the exact pressure variation is linear in Y, no zig-zagness is predicted for both $\lambda = 0$ and 0.5.

2.3.3 Compressible Flow in 2D Plane Nozzle

Figure 9 (top) shows the computational domain of a 2D convergent-divergent plane nozzle. The bottom boundary represents the axis (centreline) of the nozzle whereas the top boundary is a wall. The flow enters the left boundary and leaves through the right boundary. The total nozzle length $L = 11.56$ cm and the *throat* is midway. The half-heights of the nozzle at entry, throat and exit are 3.52 cm, 1.37 cm and 2.46 cm, respectively. The inlet Mach number is $M_{\text{in}} = 0.232$ and the exit *static* pressure is $p \,/\, p_0 = 0.1135$ where p_0 is the stagnation pressure. The stagnation enthalpy is assumed constant. For these specifications, experimental data are available [16]. This flow has been computed by Karki and Patankar [13] using curvilinear grids and Upwind Difference Scheme (UDS) for the convective terms and assuming $\mu = 0$

(that is, Euler equations are solved). Here, the flow is computed using unstructured mesh and Total Variation Diminishing (TVD) scheme [14, 17] again with $\mu = 0$.

At inflow plane, since M_{in} is known, u_{in}, T_{in} and p_{in} are specified using standard isentropic relationships [10]. In the exit plane, except for pressure (which is fixed), all other variables are linearly extrapolated from the near-exit boundary node values. At the upper nozzle wall, *tangency* condition is applied. The pressure distribution is determined by discretising a compressible flow version of the total pressure-correction equation (60). For velocities, equations for u_1, u_2 are solved and temperature is recovered from definition of stagnation enthalpy. Finally, density is determined using equation of state $p = \rho_m \, R_g \, T$. Computations are performed using 570 elements.

Figure 9 (middle) shows the predicted variations of pressure (dashed line) and Mach numbers (solid line) at the upper wall and the centreline. The experimental data (open circles) for pressure have been read from a figure in [13]. It is seen that the agreement between experiment and predictions is satisfactory. Note that the predicted Mach number at the upper wall passes through $M = 1$ exactly at the throat ($X/L = 0.5$) and reaches supersonic state $M = 2.01$ at exit. At the centreline, however, $M = 1$ location is *downstream* of the throat. Finally, Fig. 9 (bottom) shows the iso-Mach contours. Notice that the iso-Mach lines are slanted which have been found to be in agreement with computations of [13].

2.4 Main Findings

The above examples confirm our theoretical deductions (see Sect. 1.2) on importance of including simple algebraic smoothing pressure correction p'_{sm} on colocated grids to avoid prediction of zig-zag pressure. The efficacy of the smoothing correction has been shown in respect of

1. Incompressible as well as compressible flows.
2. Problems governed by parabolic and elliptic equations.
3. Problems with/without body forces.
4. Structured as well as unstructured grids.
5. Applicability to any boundary condition.

Several other applications of more complex flows can be found in [7, 11, 22, 23, 30] by way of example.

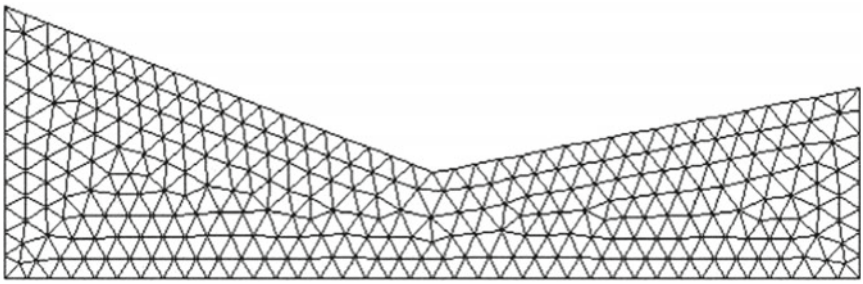

Computational Grid

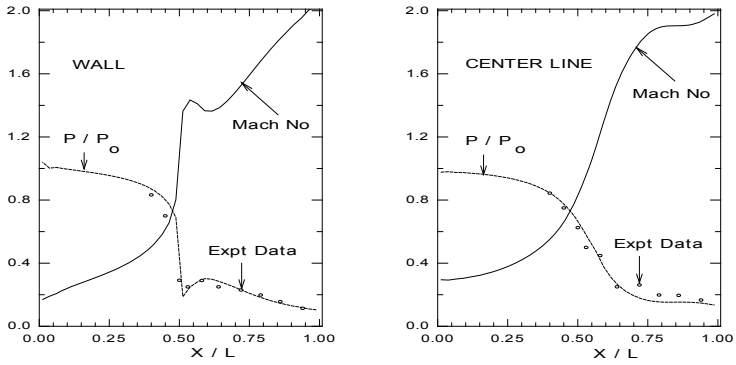

Comarison with Experimental Data [16]

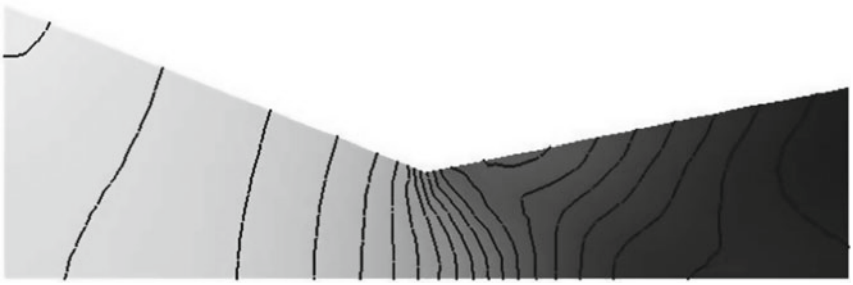

Fig. 9 2D plane nozzle: computational domain (top), variation of p and M (middle), Mach number contours 0.2 (0.1) 2.0 (bottom)

3 Interfacial Flows—Volume Error

3.1 Single-Fluid Formalism

In interfacial unsteady flows of two immiscible fluids, a problem of loss of fluid volume/mass is encountered when computing in discretised space. This problem is particularly severe when the density ratio of the two fluids is large (as, for example, in air and water). Such interfacial problems are often solved by employing *single-fluid formalism* in which the flow of two fluids is treated as that of a *single fluid* whose properties change abruptly across the interface. In such flows, the governing equations are [17]

$$\frac{\partial u_{f,j}}{\partial x_j} = \nabla \,.\, \vec{V}_f = 0 \qquad \text{(Volume Conservation)} \tag{67}$$

$$\frac{\partial(\rho_m\, u_i)}{\partial t} + \frac{\partial}{\partial x_j}\left(\rho_m\, u_{f,j}\, u_i\right) = \frac{\partial}{\partial x_j}\left[\mu_m \frac{\partial u_i}{\partial x_j}\right] - \frac{\partial p}{\partial x_i} + \rho_m\, g_i + F_{st,i} + \frac{\partial}{\partial x_j}\left[\mu_m \frac{\partial u_j}{\partial x_i}\right] \tag{68}$$

$$\frac{\partial \rho_m}{\partial t} + \frac{\partial}{\partial x_j}(\rho_m\, u_{f,j}) = 0 \qquad \text{(Mass Conservation)} \tag{69}$$

The above equations are special in that the pressure is determined from the continuity equations (67) (or volume conservation equation) but the *superficial density* ρ_m is determined from the conserved scalar equation (69) (or mass conservation equation). Thus, the equations carry characteristics of both an incompressible flow and a compressible flow. As such, incorporation of q_{disc} becomes important. Then, following from Eq. 10 and combining Eqs. 67 and 69, it can be shown that

$$\begin{aligned} p'_{sm} = q_{\text{disc}} &= \frac{1}{2}\,(p - \overline{p}) + \gamma\ \nabla\ .\, V_f \\ &= \frac{1}{2}\,(p - \overline{p}) - \frac{\gamma}{\rho_m}\left\{\frac{\partial \rho_m}{\partial t} + u_{f,j}\,\frac{\partial \rho_m}{\partial x_j}\right\} \\ &= \frac{1}{2}\,(p - \overline{p}) - \gamma\,\frac{D}{Dt}(\ln \rho_m) \end{aligned} \tag{70}$$

Notice that the last term will become significant (in the neighbourhood of the interface in discretised CFD) when density ratio of the two fluids is large. Most authors (see, for example [9, 25, 31–33]) instead of solving Eq. 69, solve an equation for *Volume Fraction F* of the heavier fluid a (say). F is defined as

$$F \equiv \frac{\rho_m - \rho_b}{\rho_a - \rho_b} \tag{71}$$

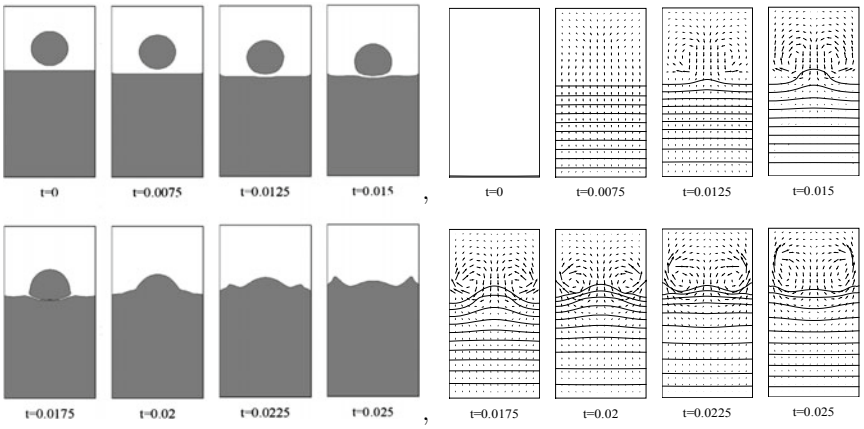

Fig. 10 Splashing of a water drop on a surface: $F = 0.5$ contours (left), pressure and velocity vectors (right)

where suffix b stands for the lighter fluid.[11] The interface is now notionally identified with $F = 0.5$. The predicted smeared (about $F = 0.5$) F-distribution at a time step is then *corrected* to conserve volume in the two-fluid CVs (in which $0 < F < 1.0$ as shown in Fig. 13-left) on the basis of *geometric* considerations. The correction procedures become extremely complex in 3D flows [25]. Other authors identify the interface with *Level Set* (usually zero) and define a level-set distance function [31]. The level-set equation is same as the F-equation but the correction procedure is invoked such that $|\nabla \cdot F| = 1$. In both procedures, apart from the additional work requirement, volume/mass balance errors arise [33].

Use of smoothing pressure correction indicated in Eq. 70, on the other hand, is very simple to implement and avoids volume/mass errors (within discretisation errors). To illustrate this, we consider few problems[12] with and without effects of surface tension.

3.2 Problems with $F_{st} = 0$

3.2.1 Splashing of a Drop on a Liquid Surface

Consider a two-dimensional rectangular enclosure (Fig. 10) of 7 mm × 14 mm dimensions. The enclosure is filled with water to a height of 8.75 mm. Initially, a cylindrical

[11] Incidentally, the superficial viscosity is now evaluated as $\mu_m = F\,\mu_a + (1 - F)\,\mu_b$.

[12] In all problems, the convective terms are discretised using a Total Variation Diminishing (TVD) scheme [14] to minimise interface smearing around $F = 0.5$. Implementation details are given in [17].

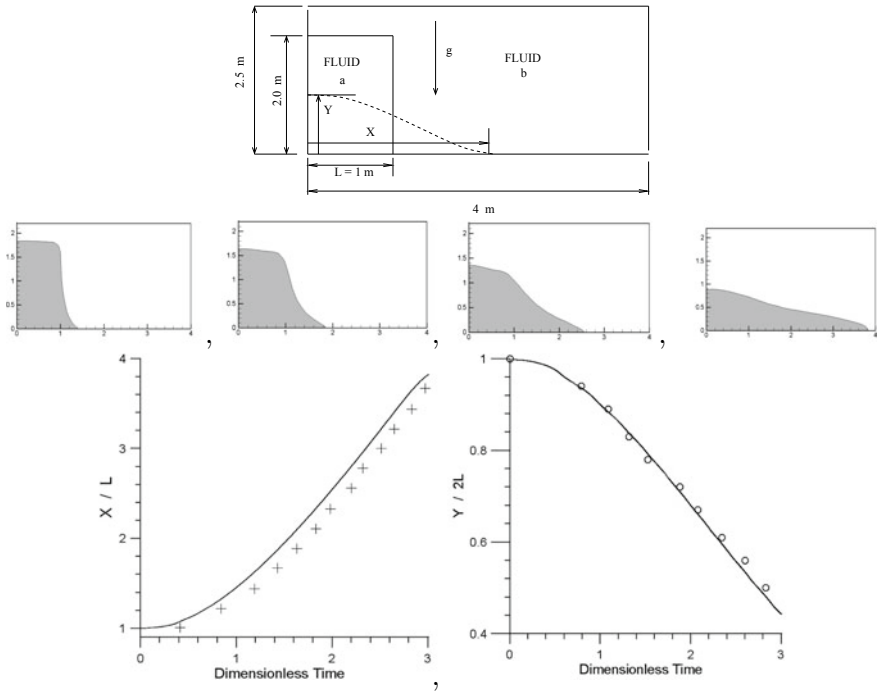

Fig. 11 Collapse of a water column

water drop of radius $r_d = 1.4$ mm is placed above the water surface in air at the centre plane $x_1 = 3.5$ mm and height $x_2 = 10.55$ mm. For $t > 0$, the drop falls under the action of gravity ($g = 9.81$ m/s^2) and splashes on the water surface creating ripples and merges with the body of water.

Computations are performed with 64 × 128 grid without exploiting symmetry. 50 iterations per time step (10^{-5} s) are required with p' under-relaxed for obtaining convergence. Computations are continued up to $t = 0.025$ s and the interface profiles ($F = 0.5$) are shown in Fig. 10 (left). The present results had maximum volume error[13] 0.002% at the last time step used in the computations. Notice also the smooth pressure prediction and the velocity vectors in Fig. 10 (right). Velocities in air have higher magnitude than in water. These motions cause development of pressure variations that deviate from pure hydrostatic pressure variation.

[13] Volume error is defined as

$$\text{Error}\ (t) = \left(\sum F_{i,j}\ \Delta V_{i,j}\right) / \left(\sum F^0_{i,j}\ \Delta V_{i,j}\right) \tag{72}$$

where F^0 is the initial F-distribution at $t = 0$ and $\Delta V_{i,j}$ is the volume of the cell surrounding node (i, j).

3.2.2 Collapse of a Water Column

Figure 11 (top) shows the problem configuration and the domain of computation. Initially, water (fluid a) column $H = 2$ m high and $L = 1$ m wide is kept at rest by means of a dam. Fluid b is air. At $t = 0$, the dam breaks resulting in collapse of water column followed by horizontal spread of water. Computations are performed with $40(x_1) \times 22(x_2)$ uniform grid. Taking $g = 9.81$, fixed time step $\Delta\tau = 0.001$ is used where $\tau = t \times (2 \times g/L)^{0.5}$. Computations are carried out till $\tau = 3$. At this time, the maximum error in volume balance was found to be 0.432%.

Figure 11 (middle) shows the $F = 0.5$ contours at $\tau = 0.9$, 1.4, 2.0 and 3.0. These contours mimic those computed by Jun and Spalding [12] using the explicit van Leer scheme [35]. Thus, the TVD scheme [14] used in present computations succeeds in sharp interface capturing. The time variations of horizontal spread X and of vertical fall Y (solid lines) are compared in Fig. 11 (bottom) with experimental data (open circles) of Martin and Moyce [15]. The comparison is reasonable notwithstanding the experimental difficulties mentioned by them.

3.2.3 Sloshing in a Tank

Figure 12 (top) shows the problem specification. The tank (40 × 25 cm) is moved with a horizontal displacement $x_1(t) = A\ \{\sin(2\pi f_1 t) - \sin(2\pi f_2 t)\}$ where $A = 7.5 \times 10^{-3}$, $f_1 = 1.598$ Hz and $f_2 = 1.307$ Hz. Computations are performed with 60×60 cells and time step $\Delta t = 0.001$ s. On all boundaries, $u_1(t) = \mathrm{d}x_1/\mathrm{d}t$, $u_2 = 0$ was specified at each time step. Nearly 500 iterations per step are required to obtain convergence. The pressure-correction equation was under-relaxed in the first 100

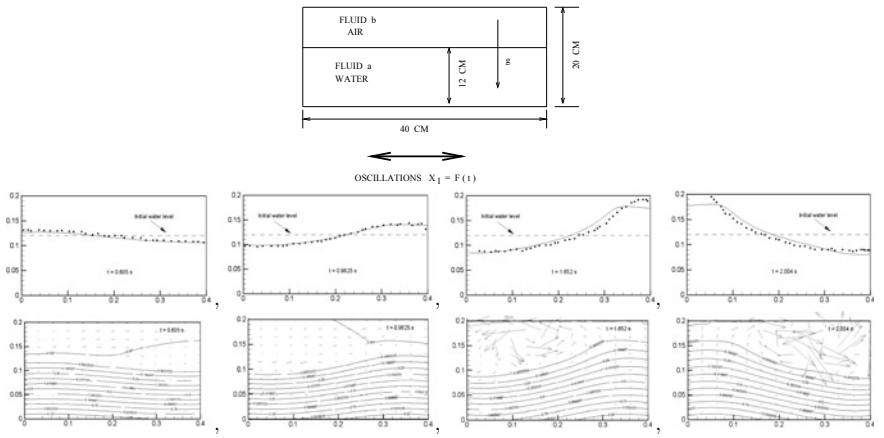

Fig. 12 Sloshing in a tank (top), interface ($F = 0.5$) locations (middle), pressure contours and velocity vectors (bottom) arrow size: 1 cm = 13 cm/s

time steps to procure convergence. At $t = 2.004$ s, the volume error (see Eq. 72) was 0.45%.

In Fig. 12 (middle), the predicted interface profiles (lines) are compared with experimental data (dots) as read from paper by Andrillon and Alessandrini [1]. Again, the agreement is seen to be reasonable. Figure 12 (bottom) shows dimensionless pressure $p^* = (p - p_{\min})/(p_{\max} - p_{\min})$ contours and velocity vectors at different times. The velocity in the air greatly exceeds that in the water. The fluid re-circulations due to interface movement accord with the expectation and the pressure contours are indeed smooth.

3.3 Problems with Finite F_{st}

In computation of many interfacial flows involving merger and splits of the interfaces, the surface tension force F_{st} is included in the momentum equations. The force acts tangent to the interface. However, the interface within a control volume is taken to be *locally* spherical. As such, the *net force* acts *normal to the interface* while the net forces normal to the interface normal cancel out. Thus, the net force per unit volume in direction i is given by [17]

$$F_{st,i} = -\sigma\,\kappa\,\frac{\partial F}{\partial x_i} = -\sigma\,\kappa\,\frac{\partial F^*}{\partial x_i} \tag{73}$$

$$\text{where} \quad F^* \equiv 0.5\left\{1 + \frac{(F - 0.5)}{|(F - 0.5)|}\right\} \tag{74}$$

where F is the volume fraction of the heavier fluid a and κ is the *interface curvature*. The replacement of F by F^* simply ensures that the surface tension force is evaluated at the interface ($F = 0.5$) only even when the F-distribution is smeared. Of course, $F_b^* = 0$ and $F_a^* = 1$.

3.3.1 Geometric Evaluation of κ

Most authors using VOF or LS methods, evaluate κ from reconstructed F-distribution as

$$\kappa = -\frac{1}{A}\left[\frac{1}{A}\,\frac{\partial F}{\partial x_i}\,\frac{\partial A}{\partial x_i} - \frac{\partial^2 F}{\partial x_i^2}\right] \quad \text{summation} \tag{75}$$

$$\text{where} \quad A = \sqrt{(\frac{\partial F}{\partial x_1})^2 + (\frac{\partial F}{\partial x_2})^2 + (\frac{\partial F}{\partial x_3})^2} \tag{76}$$

Following comments are now considered pertinent:

1. Evaluation of κ according to Eq. 75 is complex and is known to introduce discretisation errors. This has been shown by Takahira et al. [33] where a computation of a static bubble surrounded by static liquid generates spurious velocities.
2. Further, it is important to point out that many authors [2, 9, 26] study effect of surface tension coefficient σ by keeping the density and viscosity values of two fluids unchanged.[14] As such, $F_{st,i}$ calculated using Eq. 75 produces different magnitudes of the force (see Eq. 73) for the same fluid pair. However, in the literature, no real two fluid pairs having same values of density and viscosity but different values of σ are found (see, for example [21]).
3. The source of the difficulty mentioned above, however, can be traced to non-dimensionalisation of momentum equation (68). Many authors (see [33], for example) use reference velocity U, reference length L and reference properties ρ_a and μ_a to non-dimensionalise equation (68). The dimensionless equation then reads

$$\frac{\partial \rho_m^* u_i^*}{\partial t^*} + \frac{\partial \rho_m^* u_{f,j}^* u_i^*}{\partial x_j^*} = \frac{1}{Re}\frac{\partial}{\partial x_j^*}\left[\mu_m^* \frac{\partial u_i^*}{\partial x_j^*}\right] - \frac{\partial p^*}{\partial x_i^*} + \rho_m^* g_i^* - \frac{\kappa^*}{We}\frac{\partial F^*}{\partial x_i^*} + \frac{1}{Re}\frac{\partial}{\partial x_j^*}\left[\mu_m^* \frac{\partial u_j^*}{\partial x_i^*}\right] \tag{77}$$

where the dimensionless terms are

$$Re = \frac{\rho_a U L}{\mu_a} \quad \text{Reynolds number} \tag{78}$$

$$g^* = \frac{g L}{U^2} \quad \text{Froude number} \tag{79}$$

$$\kappa^* = \kappa L \quad \text{Dimensionless Curvature} \tag{80}$$

$$We = \frac{\rho_a U^2 L}{\sigma} \quad \text{Weber number} \tag{81}$$

$$\rho_m^*, \mu_m^* = \frac{\rho_m}{\rho_a}, \frac{\mu_m}{\mu_a} \quad \text{Dimensionless properties} \tag{82}$$

$$u_i^*, p^* = \frac{u_i}{U}, \frac{p}{\rho_a U^2} \quad \text{Dimensionless Velocity and Pressure} \tag{83}$$

$$x_i^*, t^* = \frac{x_i}{L}, \frac{t}{L/U} \quad \text{Dimensionless coordinates and Time} \tag{84}$$

Equation 77 thus shows that since κ^* is evaluated geometrically from F-distribution, the Weber number (We) now *appears* to be an *independent parameter* of the flow system. This interpretation leads to investigation of effect of surface tension coefficient σ (or We) for the same fluid pair. In the discussion below, we show that this is misleading and that *Weber number is not an independent parameter of the flow system.*

[14] This ignores the fact that σ is essentially a property of a specified fluid pair (a, b).

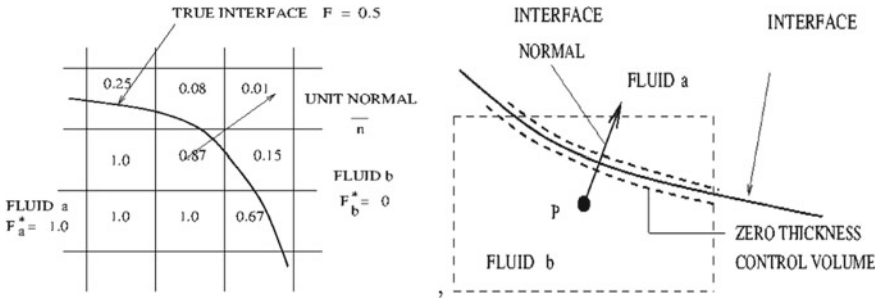

Fig. 13 Illustrative F-distribution and interface normal (left), zero-thickness CV surrounding an interface (right)

3.3.2 Fluid Dynamic Evaluation of κ

In view of the last comment, we consider an alternative approach to evaluation of κ and $F_{st,i}$. Thus, we assume that the interface is a surface of *zero thickness having no physical properties* as shown in Fig. 13 (right). Then, taking the dot product of momentum equation (68) (along with Eq. 73) with interface normal $\vec{n}$ will result in

$$\frac{\partial}{\partial n}\,(p - \tau_{nn}) = -\sigma\,\kappa\,\frac{\partial F^*}{\partial n} \qquad \rightarrow \qquad \tau_{nn} = 2\,\mu\,\frac{\partial V_n}{\partial n} \tag{85}$$

and V_n is the velocity normal to the interface. Note that the unsteady, convective and gravity terms disappear because the interface has zero thickness and no mass. However, invoking the Stokes's continuum requirement (with $q = 0$ for a control volume of zero thickness normal to the interface), we have

$$p - \tau_{nn} = \overline{p} = -\,\sigma_n \tag{86}$$

where σ_n is total normal stress. Hence, Eq. 85 will read as

$$\frac{\mathrm{d}\,\overline{p}}{\mathrm{d}\,n} = -\sigma\,\kappa\,\frac{\mathrm{d}\,F^*}{\mathrm{d}\,n} \tag{87}$$

This equation is same as the familiar Young–Laplace equation for the equilibrium of a static bubble in a static fluid in which $\tau_{nn} = 0$ [29]. Here, τ_{nn} is finite. Now, upon discretisation along the normal to the interface, it follows that (see Fig. 13 (right))

$$\sigma\,\kappa = -\,\frac{\mathrm{d}\,\overline{p}/\mathrm{d}\,n}{\mathrm{d}\,F^*/\mathrm{d}\,n} = -\,\frac{\overline{p}_b - \overline{p}_a}{F^*_b - F^*_a} = -\,\frac{\overline{p}_b - \overline{p}_a}{0 - 1} = \overline{p}_b - \overline{p}_a \tag{88}$$

and hence

$$F_{st,i} = -\left(\overline{p}_b - \overline{p}_a\right) \frac{\partial F}{\partial x_i} \tag{89}$$

This *Fluid Dynamic expression* with mean pressure difference $(\overline{p}_b - \overline{p}_a)$ on either side of the interface is again a new result. On both structured and unstructured grids, the difference of average pressures can be evaluated in the following Eq. 15:

$$\sigma\,\kappa = (\overline{p}_b - \overline{p}_a)_P = \frac{1}{3}\sum_{i=1}^{3}(\overline{p}_b - \overline{p}_a)_{x_i,P} \tag{90}$$

$$(\overline{p}_b - \overline{p}_a)_{x_i,P} = \text{solution of} \quad \frac{\partial^2}{\partial x_i^2}\left[p\,(1 - 2\,F^*)\right]_P = 0 \tag{91}$$

This manner of evaluation ensures that $\sigma\,\kappa$ is calculated at the interface ($F = 0.5$) only.

Thus, Eq. 89 evaluates the surface tension force directly from flow variables without evaluating the interface curvature. As such, the remarkable feature of this expression is that it *does not require knowledge of surface tension coefficient* σ.

3.3.3 Bursting of an Air Bubble Through Water

To demonstrate validity of two different methods of evaluating the surface tension force, we consider the bubble-burst problem (see Fig. 14). This problem has been solved by Takahira et al. [33] using the level-set method using $60 \times 60 \times 120$ grid and the surface tension force is evaluated from geometric considerations (which

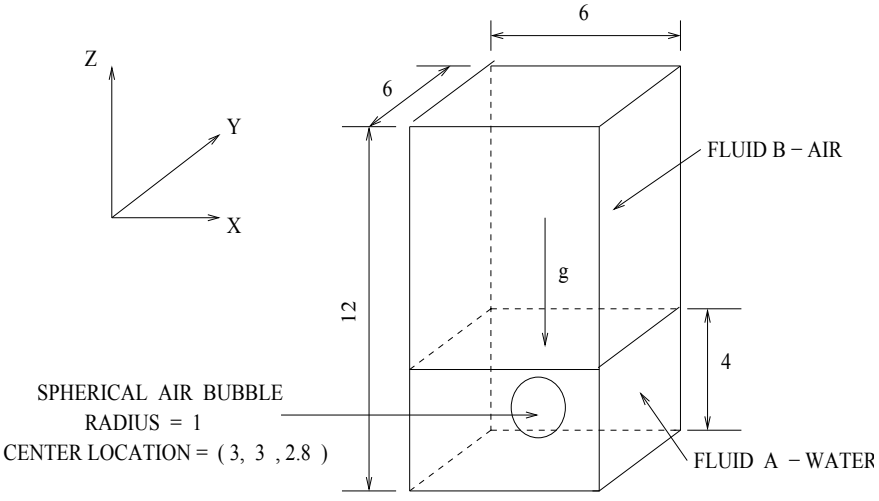

Fig. 14 Bursting of a bubble

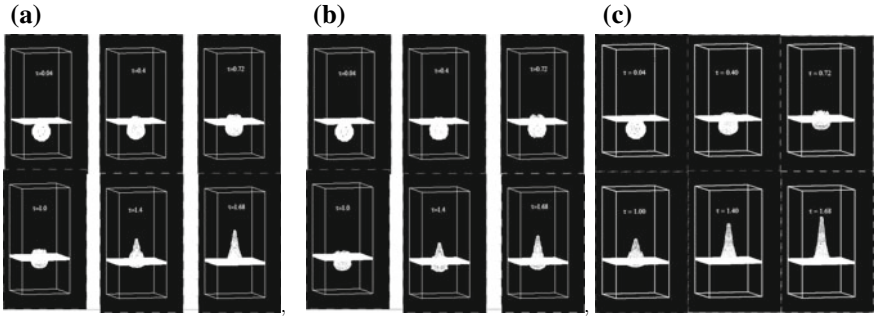

Fig. 15 Interface evolutions during bursting: **a** geometric evaluation of F_{st}, **b** fluid dynamic evaluation of F_{st}, **c** $F_{st} = 0$

requires knowledge of the value of σ). Here, in order to save computer time, the same problem is solved on coarser grid of dimensions $30 \times 30 \times 60$. Maximum of 50 iterations per time step ($\Delta\tau = 0.001$) are required to procure convergence. The reference velocity U_{ref}, properties ρ_a, μ_a and surface tension coefficient σ are chosen such that

$$Re = \frac{\rho_a \, U_{\text{ref}} \, D}{\mu_a} = 474 \qquad We = \frac{\rho_a \, U_{\text{ref}}^2 \, D}{\sigma} = 1.0$$

$$Fr = \frac{U_{\text{ref}}^2}{g \, D} = 0.64 \qquad \frac{\rho_b}{\rho_a} = 0.001 \qquad \frac{\mu_b}{\mu_a} = 0.01$$

The problem has been computed in three different ways as follows:

1. F_{st} from Eqs. 73, 75 and 76 → Fig. 15a.
2. F_{st} from Eqs. 89, 90 and 91 → Fig. 15b.
3. Ignoring surface tension force. That is, $F_{st} = 0$ → Fig. 15c.

Figure 15a, b show that predictions with both types of evaluations of F_{st} are nearly identical. The predictions also accord with the fine grid solutions obtained by [33] although the burst heights at large times are somewhat smaller due to coarseness of the grid used here. Nonetheless the formation of ripples on the liquid surface is clearly seen at $\tau = 0.4$ and 0.72. Likewise, at $\tau = 1.4$ and 1.68, formation of a *neck* in the entrained liquid suggests that a detached liquid drop is about to form.

Since predictions with both types of evaluations are nearly identical, computations are repeated with $F_{st} = 0$ (see Fig. 15c). It is seen that the burst heights are now greater indicating that the absence of surface tension force fails to minimise the interface surface during bursting, as expected.

Finally, the time variation of volume error (see Eq. 72) evaluated on coarse grid is found to increase with time in an oscillatory manner [18]. At $\tau = 1.68$, the maximum error with fluid dynamic evaluation of F_{st} is 0.078%. The same was found to be 0.093% with geometric evaluation. These errors are much smaller than the ones reported by Takahira et al. [33] on a finer grid.

Incidentally, solution to the problem of merger of two asymmetrically placed air bubbles rising in a box of square cross-section filled with water has been reported in [18]. These solutions further support the deduction that Weber number is not an independent parameter of the system.

4 Conclusions

1. Continuum requirement of Stokes's stress laws is obeyed to
   a. eliminate problem of zig-zagness pressure prediction in computation of incompressible flow on colocated grids.
   b. eliminate (within discretisation errors) the problem of loss of mass/volume at large times encountered in computation of unsteady interfacial flows.
   c. evaluate surface tension force in interfacial flows using dynamic flow variables and *without requiring knowledge of surface tension coefficient* σ.
2. Thermodynamic explanation for validity of Stokes's continuum requirement is presented with new interpretations that follow from its violations.

Acknowledgements It is a privilege for me to contribute to this volume in honour of Prof. D. B. Spalding to whom, in 2004, I sent the initial draft of my book [6] to seek his approval of the contents of the book. He not only read the draft but also gave me a task to solve a 1D problem of highly resisted flow through a porous medium. He solved the problem himself by using what he called *Date-Colocated* procedure using the PHOENICS code. Over exchange of four emails, he was satisfied that my solutions and his were in agreement. I have included with pride that 1D problem in my book. Material of section 3 was developed during sponsorship of Project No: 2005/36/47/BRNS by the Board of Research in Nuclear Science, Department of Atomic Energy, Govt of India. Contribution of Dr. Kausik Nandi, Scientist F, BARC is gratefully acknowledged.

References

1. Andrillon, Y., & Alessandrini, B. (2004). A 2D+T VOF fully coupled formulation for the calculation of breaking free-surface flow. *Journal of Marine Science and Technology, 8*, 159–168.
2. Daly, B. J. (1969). Numerical study of the effect of surface tension on interface instability. *Physics of Fluids, 17*(7), 1340–1354.
3. Date, A. W. (1998). Solution of Navier-Stokes equations on non-staggered grids at all speeds. *Numerical Heat Transfer, Part B, 33,* 451.
4. Date, A. W. (2002). SIMPLE procedure on structured and unstructured meshes with collocated variables. In *Proceedings of the 12th International Heat Transfer Conference*, Grenoble, France.
5. Date, A. W. (2004). Fluid dynamic view of pressure checker-boarding problem and smoothing pressure correction on meshes with collocated variables. *International Journal of Heat and Mass Transfer*, *48*, 4885–4898.
6. Date, A. (2005). *Introduction to computational fluid dynamics*. New York: Cambridge University Press.

7. Date, A. W. (2008). Computational fluid dynamics. In *Kirk-Othmer encyclopedia of chemical technology*, NY, USA.
8. Ferziger, J. H., & Peric, M. (1999). *Computational methods for fluid dynamics* (2nd ed.). Springer.
9. Gerlach, D., Tomar, G., Biswas, G., & Durst, F. (2005). Comparison of volume-of-fluid methods for surface tension dominant two phase flows. *International Journal of Heat and Mass Transfer, 49,* 740–754.
10. Holman, J. P. (1980). *Thermodynamics* (3rd ed.). Tokyo: McGraw-Hill Kogakusha.
11. Jagad, P. I., Puranik, B. P., & Date, A. W. (2015). A novel concept of measuring mass flow rates using flow induced stresses. *SADHANA, 40*(Part 5), 1555–1566.
12. Jun, L., & Spalding, D. B. (1988). Numerical simulation of flows with moving interfaces. *Physico-Chemical Hydrodynamics, 10,* 625–637.
13. Karki, K. C., & Patankar, S. V. (1988). A pressure based calculation procedure for viscous flows at all speeds in arbitrary configurations. In *AIAA 26th Aerospace Science Meeting,* Paper No AIAA-88-0058, Nevada, USA.
14. Lin, C. H., & Lin, C. A. (1997). Simple high-order bounded convection scheme to model discontinuities. *AIAA Journal, 35,* 563–565.
15. Martin, J. C., & Moyce, W. J. (1952). An experimental study of collapse of liquid columns on a rigid horizontal plane. *Philosophical Transactions of the Royal Society A: Mathematical, Physical and Engineering Sciences, 244,* 312–324.
16. Mason, M. L., Putnam, L. E., & Re, R. J. (1980). The effect of throat contouring on two-dimensional converging-diverging nozzles at static conditions. NASA Technical Paper, 1704.
17. Nandi, K., & Date, A. W. (2009). Formulation of fully implicit method for simulation of flows with interfaces using primitive variables. *International Journal of Heat and Mass Transfer*, *52*, 3217–3224.
18. Nandi, K., & Date, A. W. (2009). Validation of fully implicit method for simulation of flows with interfaces using primitive variables. *International Journal of Heat and Mass Transfer*, *52*, 3225–3234.
19. Patankar, S. V., & Spalding, D. B. (1971). A calculation procedure for heat mass and momentum transfer in three-dimensional parabolic flows. *International Journal of Heat and Mass Transfer*, *15*, 1787.
20. Patankar, S. V. (1981). *Numerical fluid flow and heat transfer*. NewYork: Hemisphere Publ Co.
21. Perry, R. H., & Chilton, C. H. *Chemical engineers handbook* (5th ed.). Tokyo: McGraw-Hill Kogakusha.
22. Pimpalnerkar, S., Kulkarni, M., & Date, A. W. (2005). Solution of transport equations on unstructured meshes with cell-centered collocated variables. Part II: Applications. *International Journal of Heat and Mass Transfer, 48,* 1128–1136.
23. Ray, S., & Date, A. W. (2003). Friction and heat transfer characteristics of flow through square duct with twisted tape insert. *International Journal of Heat and Mass Transfer, 46*, 889–902.
24. Rhie, C. M., & Chow, W. L. (1983). A numerical study of the turbulent flow past an isolated airfoil with trailing edge separation. *AIAA Journal*, *21*, 1525.
25. Rudman, M. (1997). Volume-tracking methods for interfacial flow calculations. *International Journal for Numerical Methods in Fluids, 24*, 671–691.
26. Salih, A., & Ghosh Moulic, S. (2006). Simulation of Rayleigh-Taylor instability using level-set method. In *33rd National and 3rd International Conference on Fluid Mechanics and Fluid Power* (p. 2006), Paper no 1303. India: IIT Bombay.
27. Sclichting. (1968). *Boundary layer theory* (English trans. Kestin J.). McGraw-Hill.
28. Shih, T. M., & Ren, A. L. (1984). Primitive variable formulations using non-staggered grid. *Numerical Heat Transfer, 7*, 413–428.
29. Shyy, W. (1994). *Computational modeling for fluid flow and interfacial transport*. Amsterdam: Elsevier.
30. Soni, B., & Date, A. W. (2011). Prediction of turbulent heat transfer in radially outward flow in twisted-tape inserted tube rotating in orthogonal mode. *Computational Thermal Science, 3*, 49–61.

31. Sussman, M., Smereka, P., & Osher, S. (1994). A level set approach for capturing solutions to incompressible two-phase flow. *Journal of Computational Physics, 114*, 146–159.
32. Sussman, M., Smith, K. M., Hussaini, M. Y., Ohta, M., & Zhi-Wei, R. (2007). A sharp interface method for incompressible two-phase flows. *Journal of Computational Physics, 221,* 469–505.
33. Takahira, H., Horiuchi, T., & Banerjee, S. (2004). An improved three dimensional level set method for gas-liquid two-phase flows. *Transaction of the ASME Journal of Fluids Engineering*, *126*, 578–585.
34. Thiart, G. D. (1990). Improved finite-difference formulation for convective-diffusive problems with SIMPLEN algorithm. *Numerical Heat Transfer, Part B, 18*, 81–95.
35. van Leer, B. (1977). Towards the ultimate conservative difference scheme IV, a new approach to numerical convection. *Journal of Computational Physics, 23*, 276–283.
36. Warsi, Z. U. A. (1993). *Fluid dynamics—Theoretical and computational approaches*. London: CRC Press.